Article

TRANSPARENT PROCESS OPEN ACCESS

THE EMBO JOURNAL

TLR sorting by Rab11 endosomes maintains intestinal epithelial-microbial homeostasis

Shiyan Yu[1], Yingchao Nie[2], Byron Knowles[3], Ryotaro Sakamori[1], Ewa Stypulkowski[1], Chirag Patel[4], Soumyashree Das[1], Veronique Douard[4], Ronaldo P Ferraris[4], Edward M Bonder[1], James R Goldenring[3], Yicktung Tony Ip[2] & Nan Gao[1,5,*]

Abstract

Compartmentalization of Toll-like receptors (TLRs) in intestinal epithelial cells (IECs) regulates distinct immune responses to microbes; however, the specific cellular machinery that controls this mechanism has not been fully identified. Here we provide genetic evidences that the recycling endosomal compartment in enterocytes maintains a homeostatic TLR9 intracellular distribution, supporting mucosal tolerance to normal microbiota. Genetic ablation of a recycling endosome resident small GTPase, *Rab11a*, a gene adjacent to a Crohn's disease risk locus, in mouse IECs and in *Drosophila* midgut caused epithelial cell-intrinsic cytokine production, inflammatory bowel phenotype, and early mortality. Unlike wild-type controls, germ-free Rab11a-deficient mouse intestines failed to tolerate the intraluminal stimulation of microbial agonists. Thus, Rab11a endosome controls intestinal host-microbial homeostasis at least partially via sorting TLRs.

Keywords enterocyte; inflammation; intestinal homeostasis; Rab11a; Toll-like receptor

Subject Categories Cell Adhesion, Polarity & Cytoskeleton; Immunology

DOI 10.15252/embj.201487888 | Received 11 January 2014 | Revised 12 June 2014 | Accepted 13 June 2014 | Published online 25 July 2014

The EMBO Journal (2014) 33: 1882–1895

Introduction

A finely tuned immuno-surveillance system that exquisitely balances immuno-responsive and immuno-repressive activities is necessary for microbe–host homeostasis in animal tissues. Genetic and environmental factors that disrupt this balance may underlie various immunological disorders including the inflammatory bowel diseases (IBDs). In mammals, the postnatal intestinal epithelial cells (IECs), after transitioning from a relatively germ-free fetal environment, immediately interact with enteric microbes and participate in immune surveillance against luminal pathogenic stimuli (Artis, 2008; Maynard *et al*, 2012). Mature human IECs appear to use specific pathogen pattern recognition receptors such as the Toll-like receptors (TLRs) to balance immune tolerance and immune response, depending on specific cellular localization of the receptors (Abreu, 2010). In cultured human colon epithelial cells, bacterial cytosine-guanine (CpG) stimulation of apically localized TLR9 from the luminal side induced tolerance to subsequent microbial agonist stimulations, whereas basolateral stimulation of TLR9 provoked NF-κB activation and cytokine production (Lee *et al*, 2006). In contrast, the exclusive basolateral localization of TLR5 in IECs appeared to facilitate this sensor to only respond to the invaded bacterial flagellin protein after barrier function impairment (Gewirtz *et al*, 2001; Rhee *et al*, 2005). Furthermore, apical localization of TLR4 was described in human colon epithelial cell lines, and this receptor changed its subcellular localization upon ligand stimulation (Cario *et al*, 2002). In the small intestine, TLR4 signaled from endosomes in response to its internalized ligand lipopolysaccharide (LPS), allowing differentiation between various types of LPS (Hornef *et al*, 2003). In addition to receptor compartmentalization, proteolytic cleavage of TLR9 in endolysosomal compartment provides another crucial control for proper receptor activation in immune cells (Ewald *et al*, 2008; Park *et al*, 2008). However, the absolute requirement of this proteolytic processing and the role of cleaved N-terminal domain for TLR9 activation are still under intensive studies (Peter *et al*, 2009; Mouchess *et al*, 2011; Onji *et al*, 2013).

Since adverse activation of microbial sensors could elicit unwanted immune responses driving intestinal pathogenesis (Leaphart *et al*, 2007; Fukata *et al*, 2011), there is a clear imperative to understand the IEC-intrinsic sorting units controlling the proper compartmentalization and activation of TLRs. A recently reported Crohn's disease risk locus at chromosome 15q22 (dbSNP ID: rs17293632) is adjacent to the human *RAB11A* (Franke *et al*, 2010). This gene encodes a small GTPase representing one of the most prominent components of a special endosomal subpopulation—the recycling endosome (Goldenring, 2013). Studies in cultured cell

1 Department of Biological Sciences, Rutgers University, Newark, NJ, USA
2 Program in Molecular Medicine, University of Massachusetts Medical School, Worcester, MA, USA
3 Experimental Surgery, Vanderbilt University Medical Center, Nashville, TN, USA
4 Department of Pharmacology and Physiology, Rutgers-New Jersey Medical School, Newark, NJ, USA
5 Rutgers Cancer Institute of New Jersey, New Brunswick, NJ, USA
*Corresponding author. Tel: +1 973 353 5523; Fax: +1 973 353 5518; E-mail: ngao@andromeda.rutgers.edu

lines suggested that the RAB11A endosome engages in intense membrane recycling and sorting, and connect the endo- and exocytic pathways (van Ijzendoorn, 2006). In cultured human colonic epithelial cells, RAB11A depletion caused abnormal lumen formation. In mouse intestines, Rab11a expression is increased in IECs during cellular differentiation and maturation (Gao & Kaestner, 2010). Here, we used genetic and biochemical approaches to show that Rab11a endosomal compartment maintains homeostatic TLR9 compartmentalization at steady-state conditions. By doing so, Rab11a appeared to prevent unwanted pro-inflammatory stimuli. Genetic and cell type-specific inactivation of Rab11a in mouse and *Drosophila* IECs midgut caused aberrant NF-κB activation, inflammatory cytokine production, and IBD phenotypes. Removal of microbial ligands (germ-free) alleviated these phenotypes in the mutants. Unlike wild-type controls, germ-free $Rab11a^{\Delta IEC}$ mice failed to tolerate intraluminal perfusion of microbial TLR agonists. Our data suggested that Rab11a controls intestinal microbial tolerance at least partially via sorting TLRs.

Results

Rab11a ablation in intestinal epithelia causes inflammation

To study the contribution of Rab11a recycling endosome to intestinal host-microbial homeostasis, we derived a *Rab11a floxed* (*fl*) conditional mouse allele. *Rab11a* global knockout mice ($Rab11a^{-/-}$) died *in utero* around the implantation stage (data not shown); therefore, we established IEC-specific *Rab11a* knockout mice ($Rab11a^{fl/fl}$; $Villin\text{-}Cre^{+}$, or $Rab11a^{\Delta IEC}$) using the Villin-Cre transgene. $Rab11a^{\Delta IEC}$ mice were born at the expected Mendelian ratio; however, at a young age, they exhibited significant runting (Fig 1A and B, see asterisk), and an approximately 40% mortality rate at the age of weaning. Male mutant mice showed higher mortality rate than their female counterparts; survivors also displayed higher mortality with aging (data not shown). Both male and female mutant mice had a dilated intestinal lumen and a shortened colon compared with their wild-type littermates (Fig 1C, see asterisks). Western blot confirmed the removal of Rab11a protein from $Rab11a^{\Delta IEC}$ mouse intestinal epithelia (Fig 1D). In contrast to control intestinal epithelia, where Rab11a was detected by immunohistochemistry in the subapical cytoplasm of villus epithelial cells (top panels, Fig 1E), Rab11a staining was absent from the $Rab11a^{\Delta IEC}$ intestinal villus epithelia (bottom panels, Fig 1E). Histopathologically, $Rab11a^{\Delta IEC}$ intestines showed blunted villi, reduced goblet cells, and macrophage infiltration into the submucosa (Fig 1F). In neonatal $Rab11a^{\Delta IEC}$ mice, the intestinal villi were frequently observed to fuse and branch (see also Supplementary Fig S1A). Pulse-chase BrdU labeling or immunostaining for phosphorylated Histone H3 (pHH3) detected increased numbers of cycling crypt cells in $Rab11a^{\Delta IEC}$ mice at all postnatal (P) stages (Fig 1G). This crypt hyperplasia was consistent with the generally enlarged crypt morphology in these mutants (Fig 1G).

Increased crypt cell proliferation was also detected when Rab11a deletion was induced in adult $Rab11a^{fl/fl}$; $Villin\text{-}CreER^{+}$ mice by tamoxifen administration (Supplementary Fig S2), suggesting that the hyperproliferative response of crypt cells might not simply be a result of defective intestinal development. Indeed, the differentiation of enterocytes and three intestinal secretory cell lineages was unaffected in $Rab11a^{\Delta IEC}$ mice (enterocytes and goblet cells shown in Fig 1F, paneth and enteroendocrine cells in Supplementary Fig S3A). Rab11a-deficient enterocytes were still capable to elaborate apical brush borders (Supplementary Fig S3B). Therefore, Rab11a deletion did not appear to disrupt the differentiation of major intestinal cell lineages. However, the epithelial hyperplasia, dysplasia, and immune cell infiltration continued to be present in older survivor $Rab11a^{\Delta IEC}$ mice (5 months old shown in Supplementary Fig S1B), which showed high histopathology scores indicative of intestinal inflammation (Fig 1H) (Adolph *et al*, 2013). Finally, tamoxifen induced deletion of Rab11a specifically in $Lgr5^{+}$ intestinal epithelial stem cells (IESCs, or crypt-based columnar cells, CBCs) in $Rab11a^{fl/fl}$; $Lgr5^{EGFP\text{-}IRES\text{-}CreER}$ mice increased the proliferation of both the $Lgr5^{+}$ and the transit-amplifying cells (Fig 1I). No immediate cell death was triggered by inducible Rab11a deletions (data not shown).

To identify the mechanisms underlying the above pathological abnormalities, we performed microarray analysis on neonatal (postnatal day 3, P3) mouse intestines using four independent pairs of RNA samples from $Rab11a^{\Delta IEC}$ and wild-type littermates (Fig 2A). Inflammatory genes encoding cytokines, chemokines, defensins, and anti-microbial peptides were significantly upregulated as the most enriched gene category in $Rab11a^{\Delta IEC}$ intestines (Fig 2B and C). Overlapping analyses revealed that 79 and 138 upregulated transcripts in $Rab11a^{\Delta IEC}$ were shared by two independent mouse enteritis models: transgenic $CD98^{IEC}$ and trinitrobenzene sulfonate (TNBS)-induced enteritis, respectively (Nguyen *et al*, 2011; Avula *et al*, 2012) (Fig 2D). These findings from microarray analysis were confirmed by quantitative real-time polymerase chain reaction (qRT-PCR) analyses, with *IL6*, *CXCL1* (human *IL8* homolog), and *CXCL5* being the most robustly activated genes (Fig 2E). A number of genes downstream of canonical Wnt pathway were not changed. Activation of IL-6 signaling pathway in $Rab11a^{\Delta IEC}$ intestines was further supported by elevated levels of phosphorylated Stat3 (pStat3), a downstream effector of IL-6 (Fig 2F). Luminescent multiplex cytokine/chemokine assays identified elevated levels of IL-6, IL-1β, and MCP1 in $Rab11a^{\Delta IEC}$ mouse serum (Fig 2G), supporting an activated systemic inflammatory response in these mice.

Professional immune cells and IECs are both capable of producing inflammatory cytokines including IL-6 (Kusugami *et al*, 1995; Vinderola *et al*, 2005). To identify the sources of these cytokines, we first performed IL-6 immunofluorescent analyses. Higher IL-6 immunoreactivities were detected in $Rab11a^{\Delta IEC}$ intestinal epithelia compared with the control epithelia (Fig 2H). The strongest IL-6 signal in wild-type epithelia was found in immune cells resident in the lamina propria (arrowheads in Fig 2H). To determine whether Rab11a-deficient IECs were the origins of observed cytokine production, we performed intestinal organoid cultures and directly measured the secreted inflammatory cytokines within the supernatant of culture medium containing live organoids (Fig 2I). After 1 week in culture, $Rab11a^{\Delta IEC}$ organoids, presumably devoid of lymphocytes, produced higher amounts of IL-6, SDF-1α/CXCL12, and IL-1β measured by ELISA (Fig 2J). Of note, even in culture, $Rab11a^{\Delta IEC}$ organoids initiated bud outgrowths more rapidly and contained a larger population of proliferative cells than wild-type organoids (Fig 2I). Therefore, the isolated $Rab11a^{\Delta IEC}$ crypts might have contained more progenitor cells to start with. Deletion of *Rab11a* in cultured $Rab11a^{fl/fl}$;$Villin\text{-}CreER^{+}$ organoids through

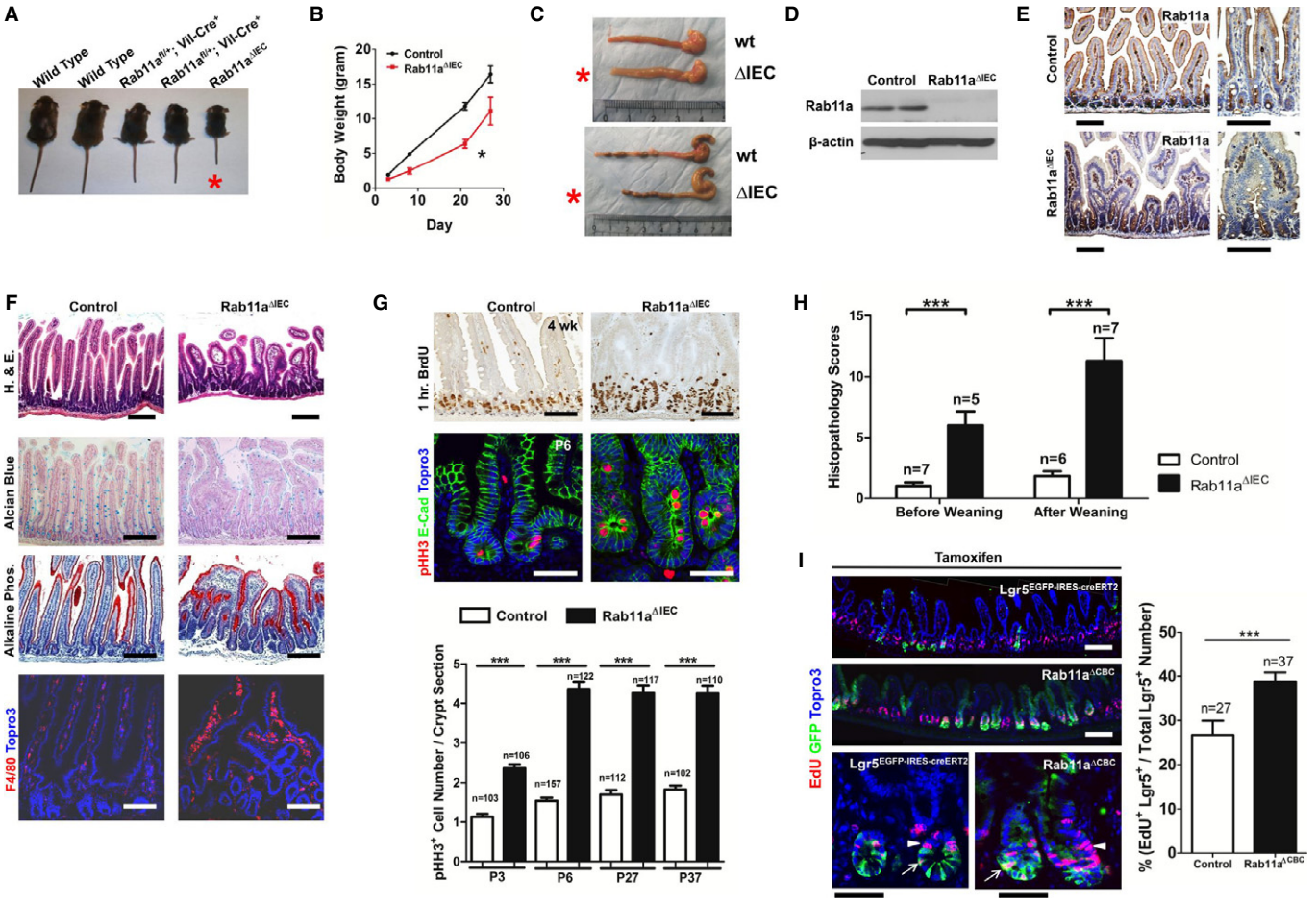

Figure 1. Rab11a ablation in mouse IECs caused enteritis.

A, B *Rab11a*$^{\Delta IEC}$ mice showed runting and postnatal growth retardation (see asterisks).

C *Rab11a*$^{\Delta IEC}$ mice (red asterisks) had dilated small intestines and shortened colons.

D Western blots confirmed Rab11a ablation.

E Immunohistochemistry confirmed Rab11a deletion in *Rab11a*$^{\Delta IEC}$ mouse IECs. In wild-type controls (top panels), Rab11a was detected in subapical cytoplasmic region. Scale bars, 10 μm.

F Early postnatal *Rab11a*$^{\Delta IEC}$ intestines contained blunted villi, reduced goblet cells, and macrophage infiltrations. Enterocytes were detected by alkaline phosphatase staining. Scale bars, 10 μm.

G BrdU labeling and pHH3 staining identified significantly increased crypt epithelial cell proliferation in *Rab11a*$^{\Delta IEC}$ intestines at all postnatal stages examined. Note that *Rab11a*$^{\Delta IEC}$ intestinal crypts were enlarged in representative 4-week-old and P6 mice. Scale bars, 10 μm. ***$P < 0.001$.

H *Rab11a*$^{\Delta IEC}$ intestines showed higher histopathology scores indicative of intestinal inflammation, compared with wild-type littermates before and after weaning. ***$P < 0.001$.

I Inducible *Rab11a* deletion in Lgr5^{+} cells caused increased proliferation in both IESCs and transit-amplifying cells. Five to 10 mice of each genotype were used in individual phenotypic analysis. Scale bars, 20 μm. ***$P < 0.001$.

administrating tamoxifen elicited a less potent increase of IL-6 secretion (Fig 2K), suggesting that loss of Rab11a triggered an epithelial cell-intrinsic cytokine production.

Rab11 depletion in *Drosophila* enterocytes caused IBD-like phenotype

The mouse *Villin* promoter-driven Rab11a deletion described above targeted all IEC cell types. It was not possible to distinguish the cell-autonomous mechanism from non-autonomous mechanism that was responsible for triggering the inflammatory responses. We employed an intestinal cell type-specific knockdown approach in *Drosophila* midgut—a tissue equivalent to mammalian intestine—using RNAi against *Rab11*, the only *Rab11a* homolog in fly genome. This system enabled us to inducibly deplete Rab11 in a particular IEC cell type via tightly controlled Gal4 drivers: the Delta promoter-Gal4 (DlGal4) for IESCs, the Su(H) binding site-Gal4 [Su(H)Gal4] for enteroblasts (EBs), the escargot promoter-Gal4 (esgGal4) for IESCs and EBs, and the Myosin1A promoter-Gal4 (Myo1AGal4) specific for enterocytes (Micchelli & Perrimon, 2006; Zeng *et al*, 2010; Jiang *et al*, 2011) (Fig 3A). Entire midguts from cell-specific Rab11 RNAi and control RNAi adult flies were analyzed for pHH3^{+} mitotic cells. Remarkably, enterocyte-specific *Rab11* knockdown, mediated by the Myo1AGal4 driver, caused the highest, nearly 100-fold, increase of mitosis in IESCs, whereas the esg and Su(H) drivers caused only modest increases of IESCs proliferation

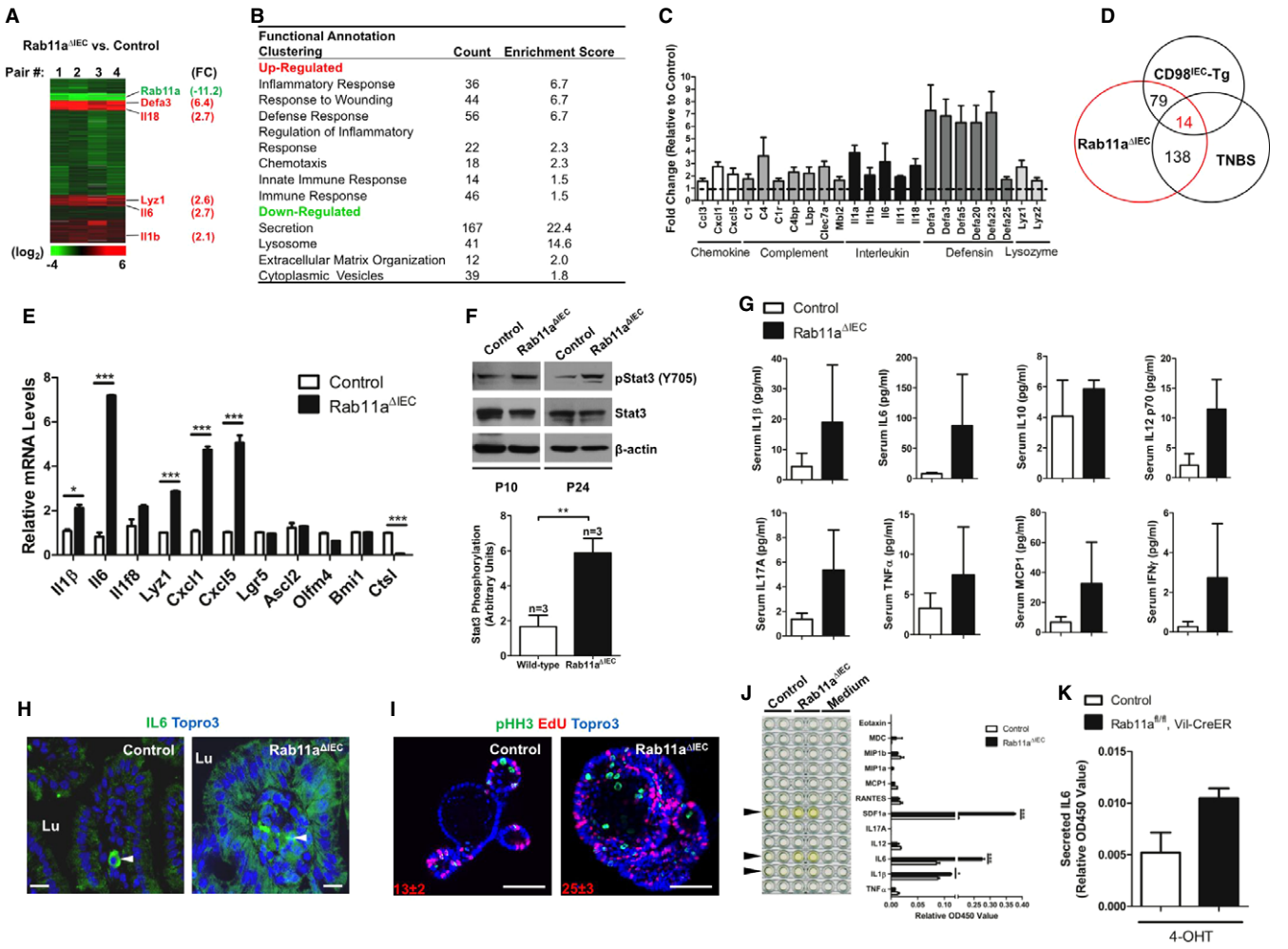

Figure 2. Rab11a-deficient IECs activated and overproduced inflammatory cytokines.

A Microarray analyses using four pairs of neonatal (P3) *Rab11a*$^{\Delta IEC}$ and wild-type littermate control intestinal samples. Upregulated inflammation-related genes clusters are shown in red, including *Defa3*, *Il18*, *Lyz1*, *Il6*, and *Il1β*, with corresponding fold changes (FC) shown relative to controls.

B Inflammation-related gene categories represented the most significantly upregulated categories in *Rab11a*$^{\Delta IEC}$ samples.

C Representative cytokines, chemokines, and anti-microbial peptides were shown to be upregulated in *Rab11a*$^{\Delta IEC}$ samples.

D 79 and 138 genes were shared by two independent mouse enteritis models.

E qRT-PCR analyses confirmed cytokine gene activations. Note that several Wnt pathway target genes, *Lgr5*, *Ascl2*, and *Olfm4*, were not changed. *$P < 0.05$, ***$P < 0.001$.

F Increased pStat3 levels in *Rab11a*$^{\Delta IEC}$ intestines. Graph represented normalized pStat3 values against total Stat3 levels, **$P <$ 0.01 for three independent mice of each genotype.

G Multiplex cytokine assays showed that *Rab11a*$^{\Delta IEC}$ mice had higher serum levels of inflammatory cytokines.

H IL-6 immunofluorescent analyses identified its overexpression by Rab11a-deficient IECs. Arrowheads point to immune cells strongly expressing IL-6 in both control and mutant tissues. *Lu*, lumen. Scale bars, 15 μm.

I The proliferative cell numbers in cultured *Rab11a*$^{\Delta IEC}$ organoids increased almost twofold, as determined by pHH3 and EdU double labeling. Scale bars, 20 μm.

J Multi-analyte cytokine ELISA detected higher levels of IL-6, IL-1β, and SDF-1α in the supernatants of *Rab11a*$^{\Delta IEC}$ organoid cultures (see arrowheads). *$P < 0.05$, ***$P < 0.001$.

K Inducible *Rab11a* deletion by tamoxifen in cultured *Rab11a*$^{fl/fl}$;*Vil-CreER* organoids induced the average IL-6 production by twofold.

(Fig 3B). In addition to the *Rab11*^{TRiP} RNAi line, two additional Rab11 RNAi lines (*Rab11*^{v22198} and *Rab11*^{v108382}) targeting distinct Rab11 sequences led to similar phenotypes after crossing with the Myo1AGal4 driver (Fig 3C), suggesting the phenotype was Rab11-specific. Epithelial organization was determined by confocal microscopy based on Myo1A-driven GFP expressed only in enterocytes and the β-catenin (Armadillo) staining that highlighted the cell membrane (Fig 3D–I). In wild-type midgut, the IESC-EB cell nests normally contained 1–2 cells (Fig 3D, arrows). However, in Myo1AGal4-driven Rab11 RNAi midguts, the nests were composed of increased number of cells (Fig 3F and H), with the *Rab11*^{v108382} line showing the strongest phenotype with the highly expanded cell nests occupying most of the gut epithelium (Fig 3H). These cell nests were expanded from Rab11 wild-type IESC as they did not contain Myo1AGal4-driven GFP. Visualized from sagittal sections, these expanded cell nests continued to occupy the basal side of the

epithelium (Fig 3E, G and I), illustrating an overall benign epithelial organization except for an increased precursor cell number due to IESC hyperproliferation. These results suggested that Rab11 depletion from enterocytes triggered neighboring IESC division, possibly through non-autonomous mechanisms.

Using qRT-PCR, we analyzed a variety of ligands and growth factors, including activators of the Wnt, JAK-STAT, and EGFR signaling pathways (Jiang & Edgar, 2012) known to be critical for IESC proliferation in adult *Drosophila* midgut. Among these factors examined, Upd3, a *Drosophila* IL-6 equivalent ligand that activates the JAK-STAT pathway (Zhou *et al*, 2013), showed the highest increase (~600-fold) in its expression comparing to controls (Fig 3J). We used an Upd3 promoter-driven lacZ reporter line (Zhou *et al*, 2013) to determine the identity of cells within the midgut that contributed to this high level of Upd3 expression. LacZ expression was markedly increased in Rab11 RNAi midguts, with a pattern identical to enterocytes that were marked by Myo1A-driven GFP (Fig 3K). Collectively, the above results from mouse intestines and *Drosophila* midgut strongly suggested that Rab11-deficient enterocytes triggered cell-autonomous cytokine productions that indirectly impacted IESC proliferation.

Activation of NF-κB and MAPK pathways in *Rab11a*$^{\Delta IEC}$ intestines

To identify the inflammatory signaling pathways that were upstream of the epithelial cytokine responses in Rab11a-deficient intestines, we analyzed NF-κB, MAPK, and JNK pathways, known to be critically involved in inflammatory and stress responses (Pasparakis, 2009; Arthur & Ley, 2013). Western blots detected significantly elevated P65 and RelB protein levels in *Rab11a*$^{\Delta IEC}$ mice at all postnatal stages, but not at fetal stages (Fig 4A). Inducible deletion of *Rab11a* in adult *Rab11a*$^{fl/fl}$*; Vil-CreER* mice by tamoxifen injection also increased the levels of P65 and RelB (Fig 4B). These changes in NF-κB protein levels likely reflected a specific response to the loss of Rab11a, as deletion of *Rab8a*, another small GTPase regulating apical membrane trafficking in IECs (Sato *et al*, 2007), did not increase P65 or RelB levels (Fig 4C). NF-κB activation in *Rab11a*$^{\Delta IEC}$ mouse intestines was also supported by elevated nuclear P65 levels from fractionated tissue lysates (Fig 4D). Abnormal activation of NF-κB was reported to cause intestinal inflammation (Zhang *et al*, 2006; Vereecke *et al*, 2010; Vlantis *et al*, 2011), similar to the phenotype of *Rab11a*$^{\Delta IEC}$ mice. Interestingly, we found that, during intestinal development in wild-type mice, P65 and RelB protein levels attenuated from late gestation stage. Rab11a levels increased during the time course, illustrating a reverse correlation (Fig 4E). Immunohistochemistry for P65 showed that postnatal *Rab11a*$^{\Delta IEC}$ intestinal villus epithelia, unlike wild-type littermates, continued to strongly express this master activator of inflammation (Ghosh & Hayden, 2008) (Fig 4F). In addition to NF-κB, activation of MAPK (Fig 4G) but not JNK pathway (data not shown) was detected in *Rab11a*$^{\Delta IEC}$ intestines, suggesting that the molecular alterations in mutant tissues did not simply reflect a generalized cell stress.

To determine whether the NF-κB pathway was required for the increased cytokine production and crypt cell proliferation, we treated *Rab11a*$^{\Delta IEC}$ organoids with an NF-κB pathway inhibitor, BAY11-0782, which irreversibly inhibits the phosphorylation of IκBα. BAY11-0782 caused significant reductions in IL-6 production and cell proliferation in *Rab11a*$^{\Delta IEC}$ organoids (Fig 4H and I). These inhibitory effects were as strong as those elicited with an IL-6 neutralizing antibody (Fig 4I). Although IL-6 recombinant proteins stimulated the proliferation of wild-type organoids, the resulting proliferative rate was still lower than *Rab11a*$^{\Delta IEC}$ organoids (Fig 4I), suggesting that additional cytokines might have also contributed to *Rab11a*$^{\Delta IEC}$ hyperplasia.

Loss of Rab11a impacted the homeostatic TLR9 intracellular distribution

As microbial sensors in IECs, TLR signaling constitutes the primary link between enteric microbes and epithelial cell-intrinsic NF-κB signaling. The elevated levels of phosphorylated Erk (Fig 4D), another mediator of TLR9 receptor signaling (Lee *et al*, 2006), and a number of downstream genes of TLR9 signaling, such as defensins and CXCL1 (Lee *et al*, 2006) (Fig 2C and E), collectively suggested that TLR9 signaling pathway might be activated in Rab11a-deficient IECs. We then explored the potential contribution of abnormal TLR signaling to the observed phenotypes. Despite a normal *TLR9* mRNA level detected by microarray and quantitative RT-PCR (Supplementary Fig S4), immunolocalization of TLR9 with a documented antibody (Lee *et al*, 2004, 2006; Tabeta *et al*, 2006; Palladino *et al*, 2007) revealed aberrant subcellular receptor aggregations that appeared to be basally (bl) shifted in Rab11a-deficient IECs (bottom panels in Fig 5A and B, and Supplementary Fig S5). Wild-type IECs contained primarily small apical (ap) TLR9 puncta in addition to weak cell surface signals (Lee *et al*, 2006) (top panels in Fig 5A and B, and Supplementary Fig S5). Close association of TLR9 aggregates with Lamp2$^+$ (Fig 5B), or with Rab7$^+$ vesicles (Supplementary Fig S5), was significantly increased in Rab11a-deficient enterocytes, suggesting that an increased amount of TLR9 was retained by endolysosomes.

Western blots for TLR9 detected altered receptor fragmentation patterns in adult *Rab11a*$^{\Delta IEC}$ intestines (male and female, right panel in Fig 5C), suggesting a changed receptor proteolytic processing. The detected multiple TLR9 fragments in wild-type intestines might reflect stepwise receptor processing by cathepsin and asparagines endopeptidase (Ewald *et al*, 2011). Using a stable *TLR9* knockdown (KD) human colonic epithelial Caco2 cell line, we validated the specificity of these endogenous TLR9 fragments (Supplementary Fig S6). This different TLR9 fragmentation pattern was absent in fetal *Rab11a*$^{\Delta IEC}$ intestines (E15.5, left panel in Fig 5C), but emerged from neonatal stages (P6: left panel in Fig 5C; 2-weeks: Fig 5D and Supplementary Fig S6), when luminal microbiota colonized the intestine. We then performed intracellular vesicle fractionation by sucrose density gradient centrifugation to determine the steady-state distribution of TLR9. In wild-type intestines, TLR9 predominantly coexisted in subcellular fractions containing Rab11a vesicles (left panel, Fig 5D); in Rab11a's absence, TLR9 distribution shifted toward fractions containing late endosome (Rab7) and lysosome (Rab9) (right panel, Fig 5D). Using co-immunoprecipitation (co-IP), we detected increased TLR9 retention by Rab7 endosomes and an elevated TLR9-MyD88 interaction in *Rab11a*$^{\Delta IEC}$ mouse intestines (see arrows, Fig 5E), supporting that in the absence of Rab11a vesicles, increased amount of TLR9 was contained by late endosome and/or lysosome, where TLR9 was reported to be processed and activated in innate immune cells (Ewald *et al*, 2008; Park *et al*,

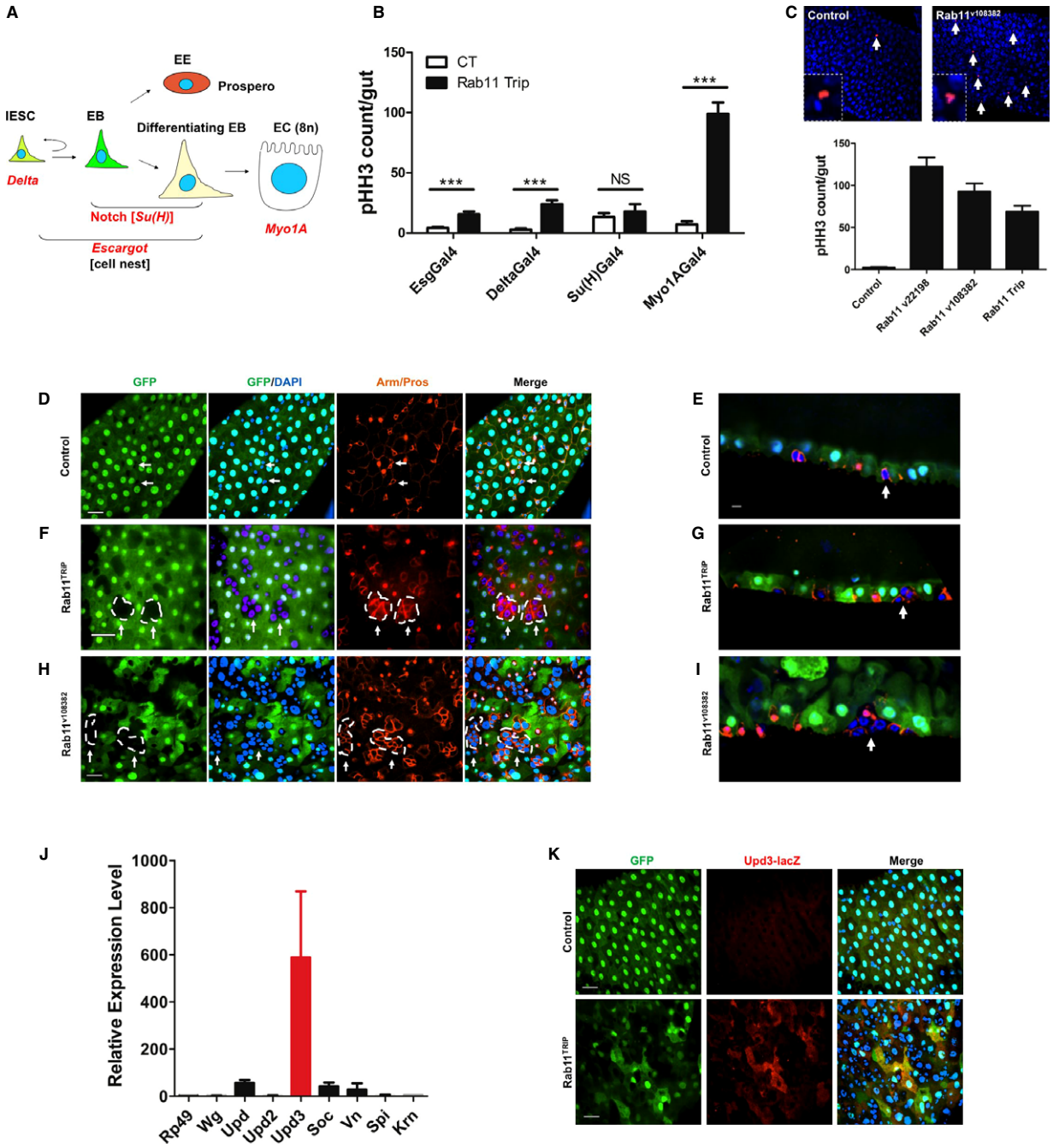

Figure 3. Inducible Rab11 depletion in *Drosophila* enterocytes caused stem cell hyperplasia and cytokine activation.

A Cell type-specific *Rab11* knockdown in *Drosophila* midguts was achieved using promoter-specific Gal4 drivers shown in red. IESC: intestinal epithelial stem cell; EB: enteroblast; EE: enteroendocrine cell; EC: enterocyte.

B Entire midguts of control RNAi and Rab11 RNAi flies were counted for $pHH3^{+}$ mitotic cells. Myo1AGal4-driven enterocyte-specific *Rab11* knockdown induced the greatest IESC division. $^{***}P < 0.001$.

C Similar phenotypes were detected in three independent Rab11 RNAi lines: v22198, v108382, and Trip, all driven by the MyolAGal4. Representative pHH3 staining is shown for v108382 Rab11 RNAi fly midgut. Arrows point to mitotic cells (red). Nuclei were stained by DAPI in blue.

D–I Confocal images of midguts from control and Rab11 RNAi flies. D, F, H are surface views; and E, G, I are sagittal views. Green cells were Myo1AGal4-driven GFP that marked enterocytes. Membrane was stained by β-catenin (Armadillo) antibody (red), nuclear red was Prospero for enteroendocrine cells, and nuclei were stained by DAPI in blue. The arrows point to IESC-EB cell nests encircled by dotted lines. Scale bars, 20 μm.

J Increased *Upd3* mRNA level was detected by qRT-PCR in Myo1AGal4-driven Rab11-depleted *Drosophila* midguts.

K Confocal images of midguts from Upd3-LacZ reporter showed undetectable *Upd3* promoter activity in control, but higher reporter activities (red) in Rab11-depleted enterocytes, which were marked by Myo1AGal4-driven GFP (green), suggesting that Rab11 depletion caused cell-autonomous Upd3 activation in enterocytes. Scale bars, 20 μm.

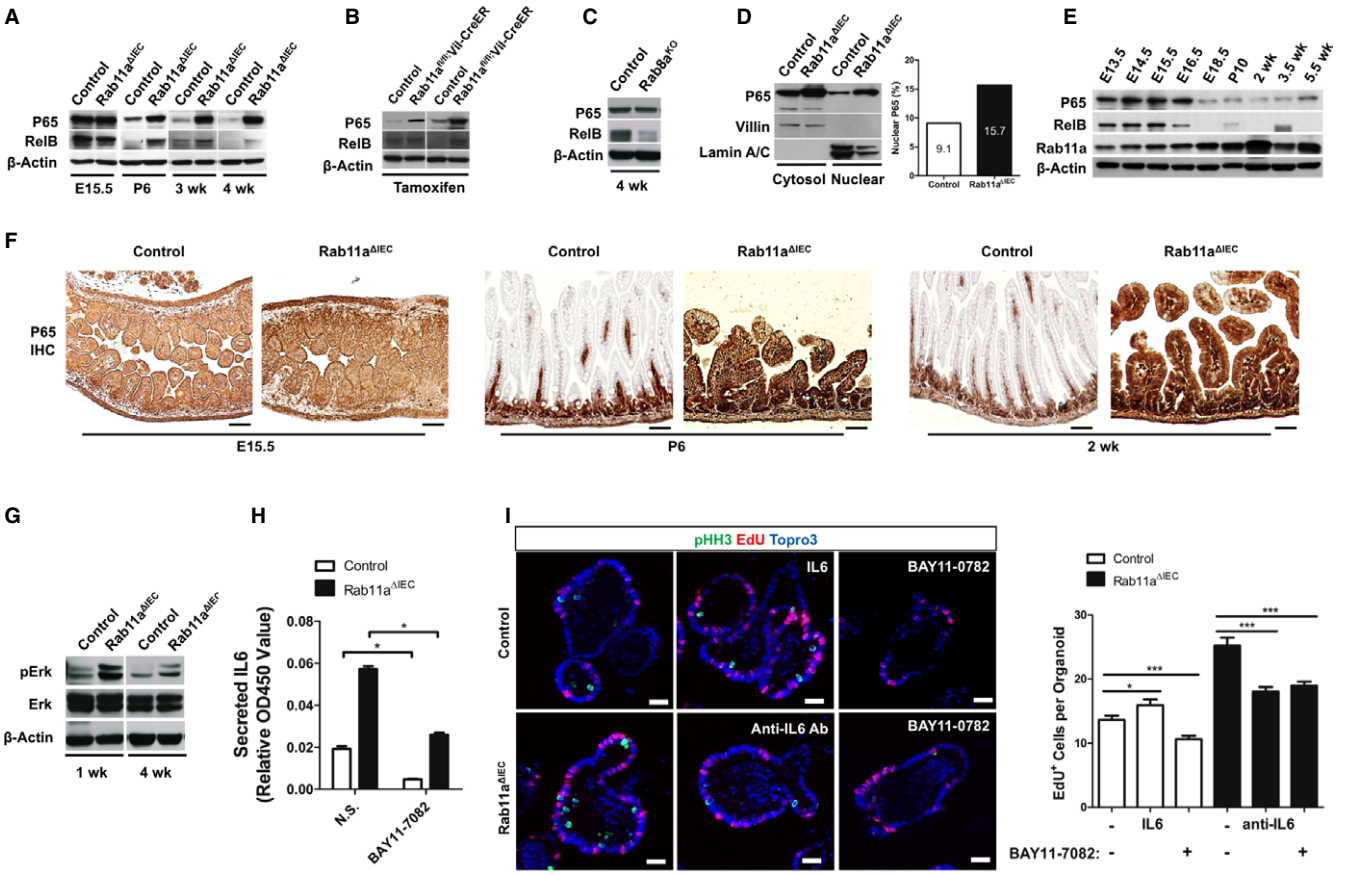

Figure 4. IEC-intrinsic activation of NF-κB and MAP kinase pathways in *Rab11a*$^{\Delta IEC}$ mice.

A P65 and RelB levels were elevated in postnatal *Rab11a*$^{\Delta IEC}$ intestines.

B Inducible Rab11a ablation in *Rab11a*$^{fl/fl}$;*Vil-CreER* mice also elevated P65 and RelB levels.

C P65 and RelB levels were not elevated in *Rab8a* knockout intestines.

D Nuclear fractionation assays determined that there was a higher level of nuclear P65 in *Rab11a*$^{\Delta IEC}$ epithelia (15.7%) than control epithelia (9.1%).

E During the development of wild-type mouse intestines, NF-κB and Rab11a levels showed reverse correlations.

F P65 level was drastically decreased in postnatal villus epithelia, but was continuously activated in postnatal *Rab11a*$^{\Delta IEC}$ epithelia. Scale bars, 20 μm.

G Levels of phosphorylated Erk were increased in *Rab11a*$^{\Delta IEC}$ mouse intestine.

H NF-κB inhibitor BAY11-7082 suppressed IL-6 production from *Rab11a*$^{\Delta IEC}$ organoids. *$P < 0.05$.

I BAY11-7082 and IL-6 neutralizing antibody suppressed the proliferation of *Rab11a*$^{\Delta IEC}$ organoids. Scale bars, 15 μm. *$P < 0.05$, ***$P < 0.001$.

2008). Additionally, when we examined adult germ-free *Rab11a*$^{\Delta IEC}$ mouse intestines where microbial TLR agonists were absent, we observed an identical pattern to the one seen in fetal intestines (Fig 5C and F). These data suggested that Rab11a critically contributed to TLR9 sorting in IECs of conventionally housed, that is, the specific pathogen free (SPF), mice.

Notably, in Caco2 cells that feature mature enterocytes (Peterson & Mooseker, 1992), TLR9 was detected by co-IP to be contained in RAB11A vesicles (Supplementary Fig S7A). Transient knockdown of *RAB11A* or treatment of cells with monensin, a recycling endosome inhibitor, caused a small but clear alteration of TLR9 fragmentation (Supplementary Fig S7B). Cell surface localization of TLR9 has been reported in both human colon epithelial cells (Lee *et al*, 2006) and mouse splenic dendritic cells (Onji *et al*, 2012). Biotinylation and membrane protein isolation assays using stable RAB11A-KD cells detected a 30% reduction of TLR9 being returned to cell surface of RAB11A-KD Caco2 cells (see arrow, Supplementary Fig S7C). In RAB11A's depletion, a sevenfold increase of TLR9 retention by RAB7$^+$ vesicles was observed in these cells (Supplementary Fig S7D), which upon forming polarized cysts, contained a larger acidic endolysosomal compartment (Fig 5G). Quantitative RT-PCR detected a 29-fold increase in *IL6* mRNA level in RAB11A-KD Caco2 cells compared to scramble KD cells (Fig 5H). These results suggested that Rab11a-mediated homeostatic TLR9 distribution might be conserved in human colonic epithelial cells.

Rab11a controls epithelial tolerance to TLR agonists

Abnormal TLR9 activation provides potential mechanism for NF-κB activation and inflammatory response observed in *Rab11a*$^{\Delta IEC}$ mice, as compartmentalization of TLR9 in IECs was reported to balance the mucosal tolerance and immune response to microbial stimulations (Wells *et al*, 2011). It was possible that *Rab11a*$^{\Delta IEC}$ intestinal epithelia were leaky causing bacterial activation of basolateral TLRs such as TLR5 (Rhee *et al*, 2005), but barrier function analyses using radioactive ^{3}H-L-glucose and ^{14}C-inulin failed to detect leakiness in

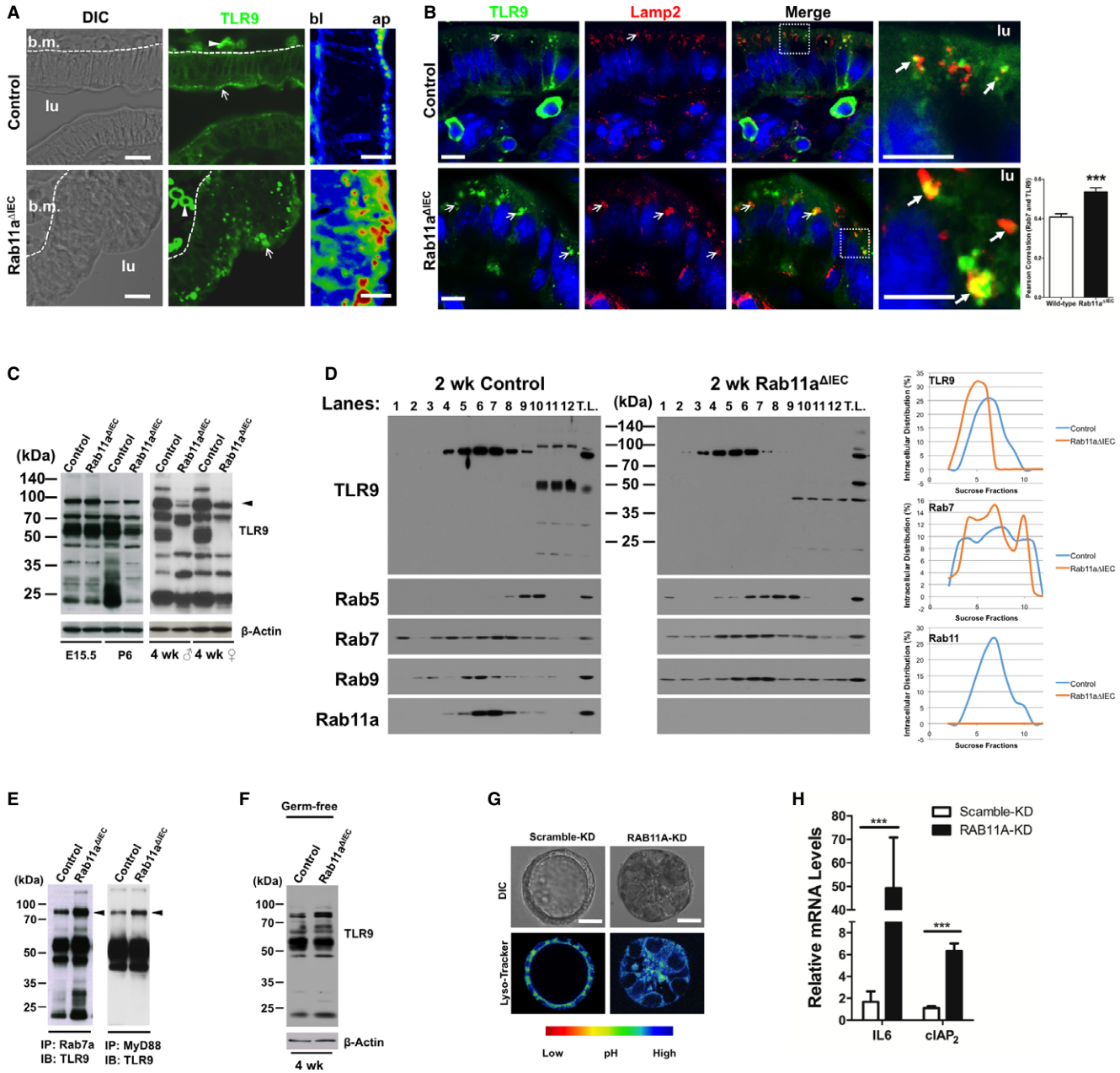

Figure 5. Rab11a deficiency impacted TLR9 distribution, fragmentation, and activation.

A Immunofluorescent staining for TLR9 (green) detected intraepithelial cell aggregations that shifted basally (bl) in Rab11a-deficient IECs. In wild-type IECs, TLR9 was detected as apical (ap) puncta, in addition to cell surface signals. lu: lumen. Scale bars, 10 μm.

B Costaining for TLR9 (green) and Lamp2 (red) showed increased TLR9 aggregations in Lamp2^{+} compartment. Arrows indicate closely associated two signals. Scale bars, 10 μm. ***$P < 0.001$.

C Western blots for TLR9 showed changed receptor fragmentation pattern in both male and female adult *Rab11a*$^{\Delta IEC}$ mice at SPF conditions. Results represent data from six mice. Note that at E15.5 fetal stage, TLR9 fragmentation pattern was similar between control and mutant intestines. Arrowhead points to an approximately 95 kDa processed TLR9. Lower molecular weight bands (< 40 kDa) may reflect non-specific proteins.

D Subcellular fractionations showed shifted TLR9 compartmentalization in *Rab11a*$^{\Delta IEC}$ toward low sucrose density fractions containing endolysosome. Lane 1–12: 0–50% sucrose fractions (see Materials and Methods). TL: total lysates. XY scatter plots illustrating percentage distribution in each sucrose fraction were generated in Excel on the basis of densitometry measurements by NIH ImageJ.

E Co-IP analyses using mouse intestinal lysates showed increased TLR9 proteins in Rab7a^{+} vesicles and elevated TLR9-MyD88 association (see arrowheads) in *Rab11a*$^{\Delta IEC}$ compared to control mice. Asterisk indicates small TLR9 fragments present in Rab7a complexes.

F TLR9 fragmentation pattern was similar between control and mutant adult mice at germ-free condition. Note that the patterns in germ-free intestines were similar to those in E15.5 intestines in (C).

G LysoTracker showed that RAB11A-KD Caco2 cysts contained larger acidic endolysosomal compartments. Rainbow color scale identifies acidic compartments as yellow. Scale bars, 15 μm.

H RAB11A-KD Caco2 cells showed increased *IL6* and *cIAP2* mRNA levels. ***$P < 0.001$.

Rab11a$^{\Delta IEC}$ epithelia, which showed rather stronger barrier function than wild-type littermates (Fig 6A), consistent with formation of apical IEC junctions in the mutants (arrows in Supplementary Fig S3B). However, germ-free *Rab11a*$^{\Delta IEC}$ mice did demonstrate an overall reduction of crypt cell proliferation (Fig 6B and C) and serum IL-6 levels (Fig 6D) compared with *Rab11a*$^{\Delta IEC}$ mice at SPF conditions. Remarkably, germ-free mutants showed reduced mortality and some became capable of breeding (data not shown). Organoids derived from germ-free *Rab11a*$^{\Delta IEC}$ mice also showed reduced *IL6* expression (Fig 6E), secreted less IL-6 proteins (Fig 6F), and proliferated less (Fig 6G). These data supported the notion that the microbial status influenced the progression of inflammatory phenotype in *Rab11a*$^{\Delta IEC}$ mouse intestines.

To determine the specific responses of germ-free *Rab11a*$^{\Delta IEC}$ intestinal epithelia to distinct TLR agonists, we performed luminal perfusion analyses in live adult mice using specific ligands for TLR9 (endotoxin-free *Escherichia coli* DNA) and TLR4 (LPS) (Fig 6H). Both wild-type and *Rab11a*$^{\Delta IEC}$ germ-free intestines responded to 4 h of *E. coli*. DNA perfusion at molecular level, showing increased levels of phosphorylated ERK, IκBα, and p38MAPK, compared with non-perfused counterparts (Fig 6I). *Rab11a*$^{\Delta IEC}$ germ-free intestines showed higher levels of ERK phosphorylation, confirming an acute and stronger activation of MAPK pathway in IECs in the absence of Rab11a. Luminal perfusion of TLR9 agonists failed to activate cytokine genes (*IL6* and *CXCL1*) in wild-type germ-free mice (Fig 6J), but drastically activated *IL6* and *CXCL1* levels (Fig 6J) in *Rab11a*$^{\Delta IEC}$ germ-free mice, suggesting that in the absence of Rab11a, IECs could not tolerate apical TLR9 ligand loading. Both wild-type and *Rab11a*$^{\Delta IEC}$ germ-free intestines responded to LPS perfusion, whereas the latter showed much more pronounced cytokine responses (Fig 6J), consistent with previous reports that the immune-suppressive function of apical TLR9 plays a role in dampening other TLR agonist stimulations (Lee *et al*, 2006). Based on these data, we proposed that Rab11a deficiency impaired IEC's tolerance to microbial TLR agonists.

Discussion

Our studies provided genetic evidence for the contribution of Rab11 endosome to intestinal host-microbial homeostasis. Using cell type-specific inducible gene ablation, we demonstrated that Rab11a-deficient mouse and *Drosophila* enterocytes activated inflammatory signaling pathways and overproduced cytokines, causing IBD phenotypes in both species. Luminal perfusion of germ-free live mouse intestines with distinct microbial TLR agonists demonstrated that Rab11a deficiency broke the mucosal tolerance to TLR agonists. These data suggested an evolutionarily conserved function of Rab11a endosomal compartment in control of intestinal host-microbial interaction.

The endosomal gene network associated with Rab11a-mediated trafficking activity is upregulated during terminal differentiation of the mouse intestinal epithelial cells (Gao & Kaestner, 2010). Expressional and functional activation of this important membrane trafficking process may reflect the increased demand by the postnatal IECs that encounter and adapt to the large microbial population after birth. At steady-state conditions in wild-type mice, the direct and constitutive recruitment and sorting of microbial sensors by Rab11a endosome may serve another important immune regulatory function dampening microbial receptor induced immune response to normal microbiota (Fig 7A). Rab11a was reported to influence cell junction *in vitro* (Wang *et al*, 2000; Desclozeaux *et al*, 2008), therefore, we initially suspected that the epithelial leakiness in these mutant mouse intestines might be an enteritis-triggering factor (Su *et al*, 2009); however, this hypothesis was ruled out by barrier function tests. Somewhat surprisingly, *Rab11a*$^{\Delta IEC}$ intestines exhibited even stronger barrier function than wild-type littermates. In fact, loss of Rab25, a member of the Rab11 subfamily also increased Claudin-1 expression and trans-epithelial resistance (Krishnan *et al*, 2013), consistent with our data suggesting that the epithelial barrier function in *Rab11a*$^{\Delta IEC}$ intestine is not impaired.

In cultured human IECs, apical versus basolateral compartmentalization of TLR9 has been linked to the distinct immune responses elicited by ligand-activated TLR9 receptors (Lee *et al*, 2006). Indeed, in our perfusion assays, wild-type germ-free mouse intestines were largely tolerant to luminal loading of purified TLR9 agonists, as no transcriptional activation of *IL6* and *CXCL1* was detected. This tolerance appeared to be TLR9-specific, since luminal LPS loading activated both genes in wild-type intestines. However, in the absence of Rab11a, luminal loading of TLR9 agonists dramatically induced *IL6* and *CDXL1* expression, suggesting that in wild-type IECs, the Rab11a vesicles suppressed TLR9 activation. Since TLR9 activation from the apical surface induced IEC tolerance to subsequent TLR agonist stimulation (Lee *et al*, 2006), complete loss of this protective mechanism in Rab11a-deficient IECs may be reflected by the strong cytokine response induced by LPS. Alternatively, Rab11a has been reported to recruit TLR4 to phagosomes activating type I interferon response in human monocytes (Husebye *et al*, 2010). We, at this moment, could not exclude the possibility of pro-inflammatory TLR4 signaling due to missorting of TLR4 in *Rab11a* knockout tissues. Abnormal TLR4 signaling was reported in cystic fibrosis model (Bruscia *et al*, 2011). As luminal perfusion of bacterial DNA did induce weak activation of Erk in wild-type intestines, we speculate that Rab11a sorting vesicles might be essential to control the strength of receptor signaling.

Endolysosomal control of TLR9 proteolysis and activation has been described in innate immune cells, but has not been well explored in IECs. Adult Rab11a-deficient IECs showed clearly altered fragmentation patterns compared to controls. In fact, independent intestines from various mutant animals, regardless of their genders, demonstrated strikingly similar fragmentation pattern to each other. This implied that, in Rab11a's absence, TLR9 was consistently transported into a certain compartment where it was improperly processed. In macrophages, the ectodomain of TLR9 is cleaved in endolysosomes for activation (Ewald *et al*, 2008; Park *et al*, 2008). Although the full-length receptor is also capable of ligand binding, only the processed TLR9 recruits MyD88 on activation (Ewald *et al*, 2008; Park *et al*, 2008). A recent study further suggested that an association between the cleaved N-terminal part and the truncated TLR9 was critical for ligand sensing and receptor activation (Onji *et al*, 2012). Rab11a deficiency impacted both TLR9 distribution and fragmentation, accompanied by increased TLR9-MyD88 association and activated TLR9 downstream targets, strongly suggesting that TLR9 was mis-activated in mutant IECs. Indeed, TLR9 recruitment into autophagosome was reported to activate MAP kinases and hypersensitivity in B cells (Chaturvedi *et al*, 2008). TLR9 transmembrane

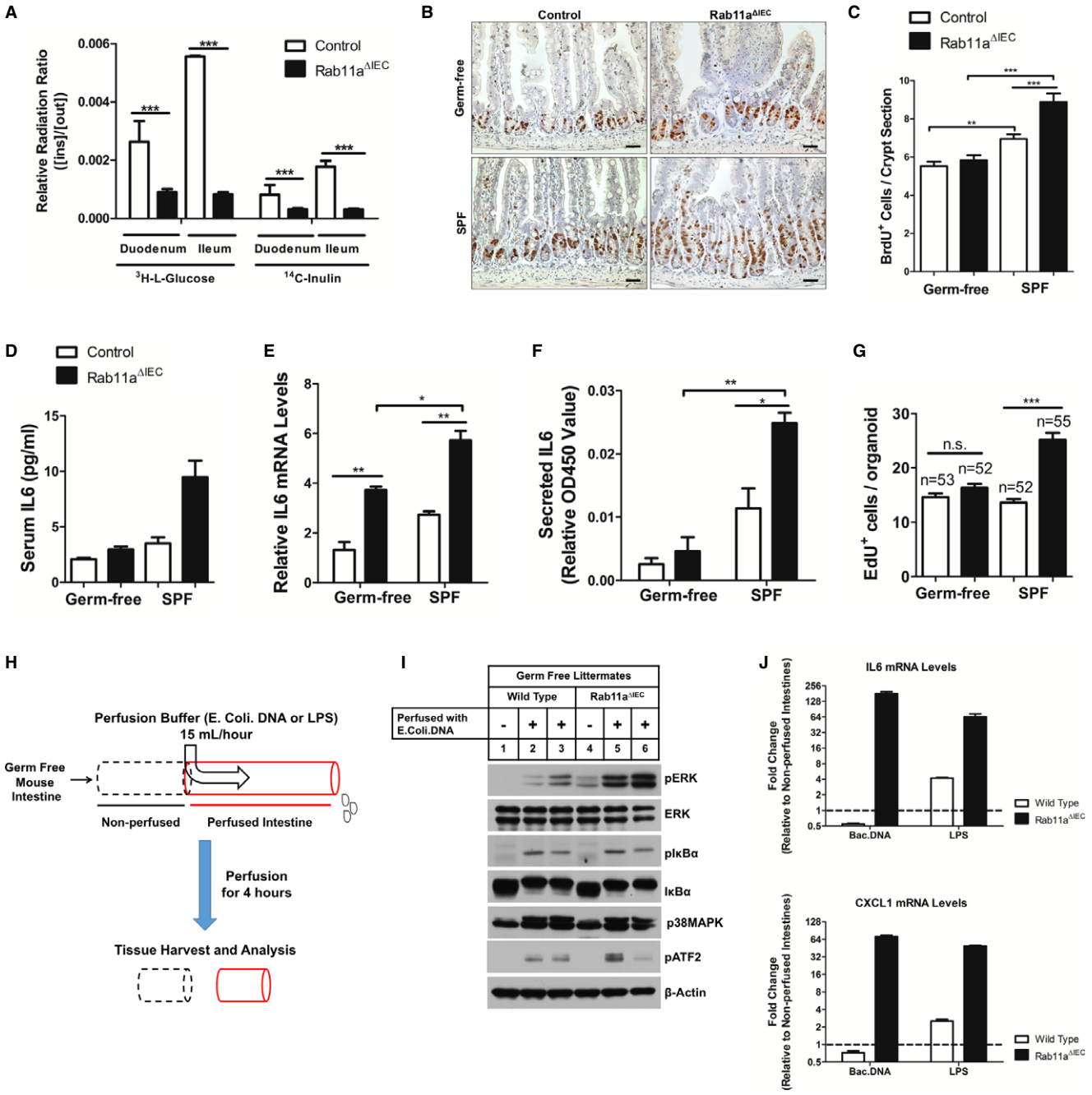

Figure 6. Rab11a controls epithelial tolerance to microbial TLR agonists.

A Barrier function tests showed that *Rab11a*$^{\Delta IEC}$ epithelia were not leaky. The active accumulation of permeabilized radioactive molecules was shown as a ratio of inside/outside quantity of ^{3}H-L-glucose or ^{14}C-inulin. *Rab11a*$^{\Delta IEC}$ duodenum and ileum showed stronger barrier function than wild-type littermates. ***$P < 0.001$.

B, C Germ-free *Rab11a*$^{\Delta IEC}$ mice showed reduced crypt hyperplasia compared to *Rab11a*$^{\Delta IEC}$ mice at SPF condition. Scale bars, 10 μm. **$P < 0.01$, ***$P < 0.001$.

D, E Germ-free *Rab11a*$^{\Delta IEC}$ mice had decreased levels of serum IL-6 and intestinal *IL6* mRNA, compared with SPF *Rab11a*$^{\Delta IEC}$ mice. *$P < 0.05$, **$P < 0.01$.

F, G *Rab11a*$^{\Delta IEC}$ organoids derived from germ-free mice showed decreased IL-6 production and reduced proliferation, compared with SPF *Rab11a*$^{\Delta IEC}$ mice. *$P < 0.05$, **$P < 0.01$, ***$P < 0.001$.

H Luminal perfusion assays, using specific TLR agonists (*E. coli* DNA or LPS), were performed on 4-week-old germ-free live animals: *Rab11a*$^{\Delta IEC}$ and wild-type littermates. After perfusion, the perfused intestinal tissues (red) and the immediately proximal non-perfused tissues (dotted black lines) were dissected for mRNA and protein analyses.

I Western blots for various signaling pathway effectors. TLR9 ligand-perfused *Rab11a*$^{\Delta IEC}$ intestines showed strong phosphorylation of ERK, compared with wild-type or non-perfused tissues.

J qRT-PCR for *IL6* and *CXCL1* was performed on TLR9 ligand-perfused wild-type and *Rab11a*$^{\Delta IEC}$ intestines. *IL6* and *CXCL1* expressional levels in corresponding non-perfused tissues were used as baselines for each genotype. Data are shown as fold inductions. Note that TLR9 ligand perfusion decreased *IL6* and *CXCL1* expressions in wild-type intestines, whereas the same perfusion induced 128-fold and 64-fold increases of *IL6* and *CXCL1* levels in *Rab11a*$^{\Delta IEC}$ intestines, respectively.

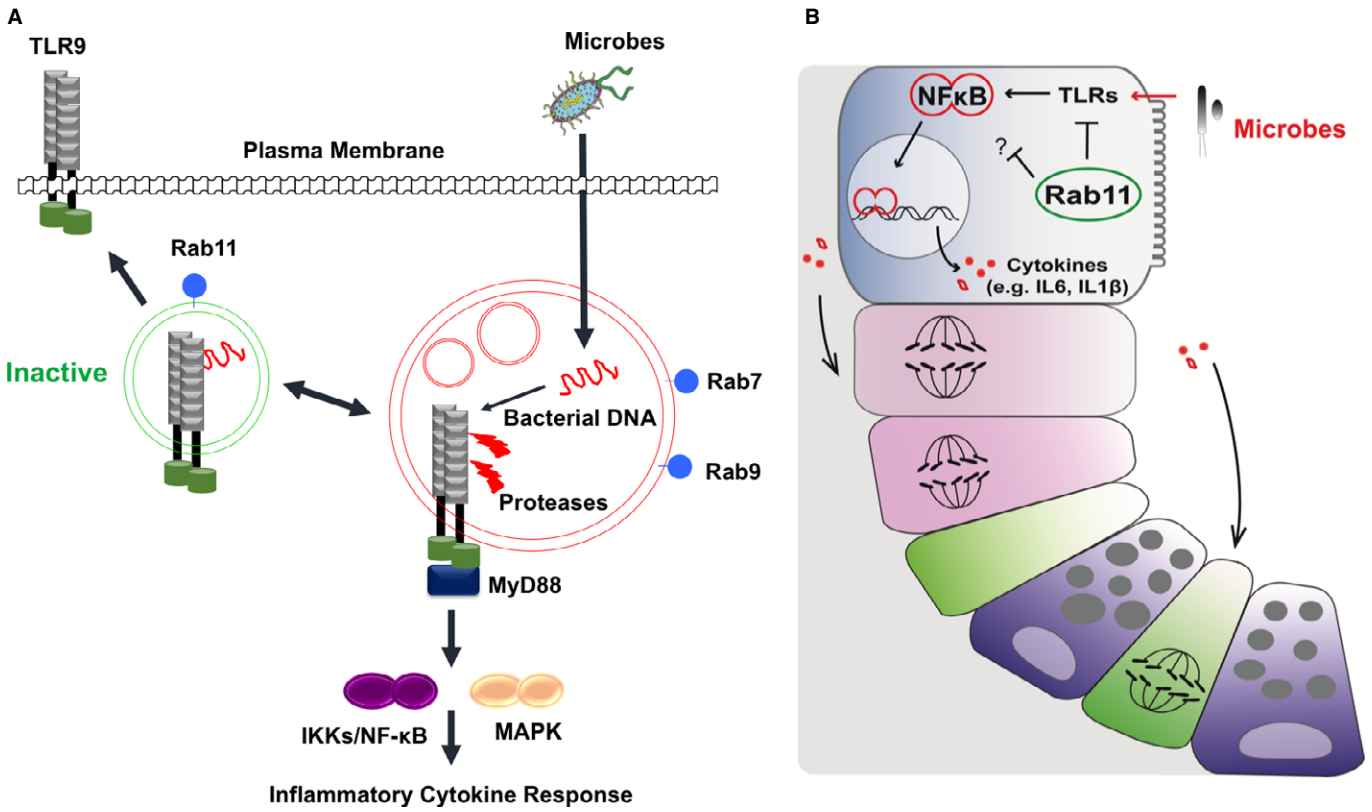

Figure 7. Rab11a vesicles in enterocytes maintain proper TLR7 compartmentalization and intestinal host-microbial homeostasis.

A At steady-state conditions, Rab11a vesicles constitutively sequester and/or recycle TLR9 to apical compartment or cell surface, dampening the receptor processing and activation in endolysosome. In the absence of Rab11a endosome, TLR9 shifts toward endolysosome promoting strong inflammatory response. Removal of microbial agonists (germ-free condition) reduces the requirement for this Rab11a-mediated immuno-suppressive function.

B Loss of Rab11 in both mouse and *Drosophila* enterocytes induced non-autonomous cell division in the IESC compartment. This enterocyte-to-stem cell signaling appears to be mediated by enterocyte-originated cytokines. The similarities shared by both animal species hinted a well-conserved Rab11a-dependent innate mechanism employed by enterocytes to support the host-microbial homeostasis.

mutations that bypass receptor proteolysis could be activated by self-DNA in dendritic cells causing lethal inflammation in mice (Mouchess *et al*, 2011). These scenarios, somewhat similar to what was observed in Rab11a-deficient IECs, suggested that intrinsic defects altering TLR9 sorting and processing could induce strong inflammatory responses. In Rab11a-deficient IECs, full activation of TLR9, still required its agonists, since complete removal of microbial agonists (in germ-free mice) alleviated inflammatory responses in these mutant mice. However, TLR9 might be the major, but unlikely the sole, microbial receptor trafficked by Rab11a vesicles in enterocytes; therefore, future work is necessary to determine the exact sorting and processing defects in TLR9 and potentially other microbial receptors. Our data at least supported the notion that, at steady-state conditions, Rab11a vesicles favored proper traffic and activation of TLR9 in host enterocytes in constant contact with microbiota (Fig 7A).

Deletion of *Rab11a* in both mouse and *Drosophila* enterocytes induced non-autonomous cell division in progenitor cell populations. This enterocyte-to-progenitor cell response was mediated by cytokines, including the highly activated IL-6 (Upd3 in *Drosophila*), derived from the mutant enterocytes (Fig 7B). The striking phenotypic and molecular similarities in both animal species indicated a well-conserved Rab11a-dependent innate mechanism employed by enterocytes to support epithelial tolerance at this microbe-rich environment. Of note, anti-IL-6 receptor antibody was effective in some patients who have active Crohn's disease (Ito *et al*, 2004). In summary, we provided the first physiological evidence for the contribution of Rab11a vesicular transport to intestinal host–microbial homeostasis.

Materials and Methods

Mice

The mouse *Rab11a* conditional floxed allele was derived through homologous recombination in mouse embryonic stem cells at a 129 genetic background. A loxP site was inserted at 242 bp downstream of *Rab11a*'s second exon, while a second loxP site introduced at 210 bp downstream of fourth exon. *Lgr5*$^{EGFP\text{-}IRES\text{-}CreERT2}$, *Vil-Cre*, *Vil-CreER*, *Rab8a* knockout mice have been described (Madison *et al*, 2002; el Marjou *et al*, 2004; Barker *et al*, 2007). Germ-free colonies were re-derived from plug mating females, housed, and bred in filtered air, autoclaved caging, bedding, food and water. Germ-free status was confirmed by PCR analyses for fecal 16rDNA. Data for mouse experiments were obtained from five to eight individual mice for each genotype group. All experiments were

performed on littermates unless otherwise stated. Additional molecular and phenotypic analyses are in the Supplementary Information and were detailed previously (Gao *et al*, 2009; Gao & Kaestner, 2010; Sakamori *et al*, 2012).

Drosophila

All *Drosophila* stocks were maintained at room temperature in yeast extract/cornmeal/molasses/agar food medium. w^{1118} were used as the wild-type for crossing with various Gal4 lines for control experiments. The fly stocks $Rab11^{TRiP}$ was originated from Transgenic RNAi Project of Harvard Medical School and obtained from Bloomington (#27730). The $Rab11^{v22198}$ and $Rab11^{v108392}$ were obtained from Vienna Drosophila RNAi Center. The Gal4 drivers have been described previously (Micchelli & Perrimon, 2006; Zeng *et al*, 2010; Jiang *et al*, 2011). The Upd3-LacZ was as described (Zhou *et al*, 2013). Control flies were crosses between w^- and the Gal4 lines as indicated. All fly crosses also contained the tubulin-$Gal80^{ts}$ for temporal control, and 5- to 7-day-old flies were shifted to 29°C for 4 days to allow Gal4 activity and RNAi.

Mouse intestinal crypt isolation and organoid culture

Procedures for crypt isolation and organoid culture were essentially the same as reported (Sato *et al*, 2009). Crypts were counted, resuspended in Matrigel (BD Biosciences, #354234), and seeded into 8-well chamber slides, 48-well or 24-well culture plates, depending on the purpose of the study. After Matrigel polymerization, crypt culture medium (Advanced DMEM/F12 containing 50 ng/ml recombinant murine EGF, 1 μg/ml recombinant murine R-Spondin 1, 100 ng/ml recombinant murine Noggin, 1× N2 supplement, 1× B27 supplement, 1 mM *N*-acetylcysteine, 2 mM GlutaMax, 10 mM HEPES, and 100 U/ml penicillin/100 mg/ml streptomycin) was applied. For *in vitro* treatment of organoids, 200 crypts/wells were seeded in replicates for each genotype. After formation of control and mutant organoids, fresh medium was replaced containing recombinant mouse IL-6 (100 ng/ml), IL-6 neutralizing antibody (1 μg/ml), BAY11-0782 (10 μM), or no supplement. After 24 h, the cultures were used either for cytokine ELISA or for immunofluorescent analyses detailed in Supplementary Information. All assays were independently repeated at least three times.

Histopathology scoring of intestinal inflammation

To assess the inflammation of small intestine, a histological scoring system as described previously (Adolph *et al*, 2013) was conducted on operator blinded histology sections. Briefly, this histological scoring system comprised five histological features which were evaluated semi-quantitatively (0, absent; 1, mild; 2, moderate; 3, severe): mononuclear cell infiltrate (0–3), crypt hyperplasia (0–3), epithelial injury/erosion (0–3), polymorphonuclear cell infiltrates (0–3), and transmural inflammation (0, absent; 1, submucosal; 2, one focus extending into muscularis and serosa; 3, up to five foci extending into muscularis and serosa; 4, diffuse). In addition, one extended factor was derived based on the fraction of bowel length involved by inflammation: (i) < 10%; (ii) 10–25%; (iii) 25–50%; and (iv) > 50%. The histological score was calculated as a sum of five independent parameters multiplied by the extended factor.

Sucrose density gradient centrifugation

Procedures were modified from Yao *et al* (2009). Small intestinal tissues were suspended in cold detergent-free lysis buffer (100 mM sodium carbonate pH 11, 0.5 mM EDTA, 1 mM phenylmethanesulfonyl fluoride and 2× protease inhibitor (Roche Diagnostics) and lysed with 50 strokes using tight pestle in glass homogenizer. Homogenates were centrifuged at 3,000 *g* for 10 min at 4°C to remove nuclei, large cell debris and unbroken cells. The supernatants were adjusted to 50% sucrose by mixing with 90% (w/v) sucrose solution (in 25 mM 4-Morpholineethanesulfonic acid, 150 mM NaCl, 250 mM $NaCO_3$), and loaded to the bottom of 12.5-ml ultracentrifugation tube. Eleven discontinuous sucrose gradients (40, 35, 25, 22.5, 20, 17.5, 15, 12.5, 10 and 5%, and homogenizing buffer) were sequentially layered on top of the lysates. After centrifugation at 100,000 *g* for 16 h in SW40Ti swinging-bucket rotor (Beckman) at 4°C, 12 fractions, 1 ml of each layer, were collected and stored at −80°C. Twenty microlitre of each fraction as well as total tissue lysates were denatured and subjected to Western blots.

Intraluminal perfusion assay

To examine the response of small intestine to specific TLR9 agonist *in vivo*, mice were anesthetized intraperitoneally with 60 mg/kg ketamine and 5 mg/kg xylazine initially, and subjected to midline laparotomy for exposure of the entire small intestine with intact blood vessels and nerve connections. Two small incisions were made at the proximal end of jejunum and the distal end of ileum, respectively. Catheters were inserted, secured with surgical thread, and connected to an inflow polyethylene tube. After the contents were flashed, the small intestine was continuously perfused from jejunum to ileum with KRB buffer containing 8 μg/ml of *E. coli* ssDNA (Invivogen, Catalog #tlrl-ssec) or 2 μg/ml of LPS (Sigma, Catalog #L4391) at a rate of 15 ml/h using a peristaltic pump for 4 h and then harvested for further analysis. The temperature of mouse body and perfusion solution was maintained at 37°C by heating pads/heat lamps and water bath, respectively.

Statistical analysis

Data are presented as mean values of 3–6 independently replicated experiments, with error bars representing standard error of the mean (SEM). A two-tailed Student's *t*-test was used to determine significance of differences. Co-localization of dual fluorescent signals was deduced from confocal microscopic images using Pearson correlation analyses (Bolte & Cordelieres, 2006). Significance was indicated as "*" when *P*-value < 0.05, "**" $P < 0.01$, and "***" $P < 0.001$.

Supplementary information for this article is available online: http://emboj.embopress.org

Acknowledgements

The authors thank Dr. Qiang Feng and Pavan Vedula for helps with some graphic illustration and data analyses. This work was supported by National Institute of Health (NIH) Grants DK085194, DK093809, DK102934, and CA178599 to N.G.; DK48370 and DK070856 to J.R.G.; DK83450 to Y.T.I.; Charles

and Johanna Busch Memorial Award (659160) and Rutgers Faculty Research Grant (281708) to N.G. Y.T.I. is a member of the UMass DERC (DK32520), the UMass Center for Clinical and Translational Science (UL1TR000161) and the Guangdong Innovative Research Team Program (No. 201001Y0104789252); S.Y. is supported by New Jersey Commission on Cancer Research Postdoctoral Fellowship (DFHS13PPC016).

Author contributions

SY, EMB, JRG, TI, and NG conceived the project, designed experiments, and analyzed data; SY, YN, BK, RS, ES, CP, SD, RPF, and VD performed experiments and analyzed data; SY, TI, and NG wrote the paper.

Conflict of interest

The authors declare that they have no conflict of interest.

References

Abreu MT (2010) Toll-like receptor signalling in the intestinal epithelium: how bacterial recognition shapes intestinal function. *Nat Rev Immunol* 10: 131 – 144

Adolph TE, Tomczak MF, Niederreiter L, Ko HJ, Bock J, Martinez-Naves E, Glickman JN, Tschurtschenthaler M, Hartwig J, Hosomi S, Flak MB, Cusick JL, Kohno K, Iwawaki T, Billmann-Born S, Raine T, Bharti R, Lucius R, Kweon MN, Marciniak SJ *et al* (2013) Paneth cells as a site of origin for intestinal inflammation. *Nature* 503: 272 – 276

Arthur JS, Ley SC (2013) Mitogen-activated protein kinases in innate immunity. *Nat Rev Immunol* 13: 679 – 692

Artis D (2008) Epithelial-cell recognition of commensal bacteria and maintenance of immune homeostasis in the gut. *Nat Rev Immunol* 8: 411 – 420

Avula LR, Knapen D, Buckinx R, Vergauwen L, Adriaensen D, Van Nassauw L, Timmermans JP (2012) Whole-genome microarray analysis and functional characterization reveal distinct gene expression profiles and patterns in two mouse models of ileal inflammation. *BMC Genomics* 13: 377

Barker N, van Es JH, Kuipers J, Kujala P, van den Born M, Cozijnsen M, Haegebarth A, Korving J, Begthel H, Peters PJ, Clevers H (2007) Identification of stem cells in small intestine and colon by marker gene Lgr5. *Nature* 449: 1003 – 1007

Bolte S, Cordelieres FP (2006) A guided tour into subcellular colocalization analysis in light microscopy. *J Microsc* 224(Pt 3): 213 – 232

Bruscia EM, Zhang PX, Satoh A, Caputo C, Medzhitov R, Shenoy A, Egan ME, Krause DS (2011) Abnormal trafficking and degradation of TLR4 underlie the elevated inflammatory response in cystic fibrosis. *J Immunol* 186: 6990 – 6998

Cario E, Brown D, McKee M, Lynch-Devaney K, Gerken G, Podolsky DK (2002) Commensal-associated molecular patterns induce selective toll-like receptor-trafficking from apical membrane to cytoplasmic compartments in polarized intestinal epithelium. *Am J Pathol* 160: 165 – 173

Chaturvedi A, Dorward D, Pierce SK (2008) The B cell receptor governs the subcellular location of Toll-like receptor 9 leading to hyperresponses to DNA-containing antigens. *Immunity* 28: 799 – 809

Desclozeaux M, Venturato J, Wylie FG, Kay JG, Joseph SR, Le HT, Stow JL (2008) Active Rab11 and functional recycling endosome are required for E-cadherin trafficking and lumen formation during epithelial morphogenesis. *Am J Physiol Cell Physiol* 295: C545 – C556

Ewald SE, Lee BL, Lau L, Wickliffe KE, Shi GP, Chapman HA, Barton GM (2008) The ectodomain of Toll-like receptor 9 is cleaved to generate a functional receptor. *Nature* 456: 658 – 662

Ewald SE, Engel A, Lee J, Wang M, Bogyo M, Barton GM (2011) Nucleic acid recognition by Toll-like receptors is coupled to stepwise processing by cathepsins and asparagine endopeptidase. *J Exp Med* 208: 643 – 651

Franke A, McGovern DP, Barrett JC, Wang K, Radford-Smith GL, Ahmad T, Lees CW, Balschun T, Lee J, Roberts R, Anderson CA, Bis JC, Bumpstead S, Ellinghaus D, Festen EM, Georges M, Green T, Haritunians T, Jostins L, Latiano A *et al* (2010) Genome-wide meta-analysis increases to 71 the number of confirmed Crohn's disease susceptibility loci. *Nat Genet* 42: 1118 – 1125

Fukata M, Shang L, Santaolalla R, Sotolongo J, Pastorini C, Espana C, Ungaro R, Harpaz N, Cooper HS, Elson G, Kosco-Vilbois M, Zaias J, Perez MT, Mayer L, Vamadevan AS, Lira SA, Abreu MT (2011) Constitutive activation of epithelial TLR4 augments inflammatory responses to mucosal injury and drives colitis-associated tumorigenesis. *Inflamm Bowel Dis* 17: 1464 – 1473

Gao N, White P, Kaestner KH (2009) Establishment of intestinal identity and epithelial-mesenchymal signaling by Cdx2. *Dev Cell* 16: 588 – 599

Gao N, Kaestner KH (2010) Cdx2 regulates endo-lysosomal function and epithelial cell polarity. *Genes Dev* 24: 1295 – 1305

Gewirtz AT, Navas TA, Lyons S, Godowski PJ, Madara JL (2001) Cutting edge: bacterial flagellin activates basolaterally expressed TLR5 to induce epithelial proinflammatory gene expression. *J Immunol* 167: 1882 – 1885

Ghosh S, Hayden MS (2008) New regulators of NF-kappaB in inflammation. *Nat Rev Immunol* 8: 837 – 848

Goldenring JR (2013) A central role for vesicle trafficking in epithelial neoplasia: intracellular highways to carcinogenesis. *Nat Rev Cancer* 13: 813 – 820

Hornef MW, Normark BH, Vandewalle A, Normark S (2003) Intracellular recognition of lipopolysaccharide by toll-like receptor 4 in intestinal epithelial cells. *J Exp Med* 198: 1225 – 1235

Husebye H, Aune MH, Stenvik J, Samstad E, Skjeldal F, Halaas O, Nilsen NJ, Stenmark H, Latz E, Lien E, Mollnes TE, Bakke O, Espevik T (2010) The Rab11a GTPase controls toll-like receptor 4-induced activation of interferon regulatory factor-3 on phagosomes. *Immunity* 33: 583 – 596

van Ijzendoorn SC (2006) Recycling endosomes. *J Cell Sci* 119(Pt 9): 1679 – 1681

Ito H, Takazoe M, Fukuda Y, Hibi T, Kusugami K, Andoh A, Matsumoto T, Yamamura T, Azuma J, Nishimoto N, Yoshizaki K, Shimoyama T, Kishimoto T (2004) A pilot randomized trial of a human anti-interleukin-6 receptor monoclonal antibody in active Crohn's disease. *Gastroenterology* 126: 989 – 996; discussion 947

Jiang H, Grenley MO, Bravo MJ, Blumhagen RZ, Edgar BA (2011) EGFR/Ras/MAPK signaling mediates adult midgut epithelial homeostasis and regeneration in *Drosophila*. *Cell Stem Cell* 8: 84 – 95

Jiang H, Edgar BA (2012) Intestinal stem cell function in *Drosophila* and mice. *Curr Opin Genet Dev* 22: 354 – 360

Krishnan M, Lapierre LA, Knowles BC, Goldenring JR (2013) Rab25 regulates integrin expression in polarized colonic epithelial cells. *Mol Biol Cell* 24: 818 – 831

Kusugami K, Fukatsu A, Tanimoto M, Shinoda M, Haruta J, Kuroiwa A, Ina K, Kanayama K, Ando T, Matsuura T, Yamaguchi T, Morisa K, Ieda M, Iokawa H, Ishihara A, Sarai S (1995) Elevation of interleukin-6 in inflammatory bowel disease is macrophage- and epithelial cell-dependent. *Dig Dis Sci* 40: 949 – 959

Leaphart CL, Cavallo J, Gribar SC, Cetin S, Li J, Branca MF, Dubowski TD, Sodhi CP, Hackam DJ (2007) A critical role for TLR4 in the pathogenesis of necrotizing enterocolitis by modulating intestinal injury and repair. *J Immunol* 179: 4808 – 4820

Lee HK, Dunzendorfer S, Tobias PS (2004) Cytoplasmic domain-mediated dimerizations of toll-like receptor 4 observed by beta-lactamase enzyme fragment complementation. *J Biol Chem* 279: 10564 – 10574

Lee J, Mo JH, Katakura K, Alkalay I, Rucker AN, Liu YT, Lee HK, Shen C, Cojocaru G, Shenouda S, Kagnoff M, Eckmann L, Ben-Neriah Y, Raz E (2006) Maintenance of colonic homeostasis by distinctive apical TLR9 signalling in intestinal epithelial cells. *Nat Cell Biol* 8: 1327 – 1336

Madison BB, Dunbar L, Qiao XT, Braunstein K, Braunstein E, Gumucio DL (2002) Cis elements of the villin gene control expression in restricted domains of the vertical (crypt) and horizontal (duodenum, cecum) axes of the intestine. *J Biol Chem* 277: 33275 – 33283

el Marjou F, Janssen KP, Chang BH, Li M, Hindie V, Chan L, Louvard D, Chambon P, Metzger D, Robine S (2004) Tissue-specific and inducible Cre-mediated recombination in the gut epithelium. *Genesis* 39: 186 – 193

Maynard CL, Elson CO, Hatton RD, Weaver CT (2012) Reciprocal interactions of the intestinal microbiota and immune system. *Nature* 489: 231 – 241

Micchelli CA, Perrimon N (2006) Evidence that stem cells reside in the adult *Drosophila* midgut epithelium. *Nature* 439: 475 – 479

Mouchess ML, Arpaia N, Souza G, Barbalat R, Ewald SE, Lau L, Barton GM (2011) Transmembrane mutations in Toll-like receptor 9 bypass the requirement for ectodomain proteolysis and induce fatal inflammation. *Immunity* 35: 721 – 732

Nguyen HT, Dalmasso G, Torkvist L, Halfvarson J, Yan Y, Laroui H, Shmerling D, Tallone T, D'Amato M, Sitaraman SV, Merlin D (2011) CD98 expression modulates intestinal homeostasis, inflammation, and colitis-associated cancer in mice. *J Clin Invest* 121: 1733 – 1747

Onji M, Kanno A, Saitoh S, Fukui R, Motoi Y, Shibata T, Matsumoto F, Lamichhane A, Sato S, Kiyono H, Yamamoto K, Miyake K (2012) An essential role for the N-terminal fragment of Toll-like receptor 9 in DNA sensing. *Nat Commun* 4: 1949

Onji M, Kanno A, Saitoh S, Fukui R, Motoi Y, Shibata T, Matsumoto F, Lamichhane A, Sato S, Kiyono H, Yamamoto K, Miyake K (2013) An essential role for the N-terminal fragment of Toll-like receptor 9 in DNA sensing. *Nat Commun* 4: 1949

Palladino MA, Johnson TA, Gupta R, Chapman JL, Ojha P (2007) Members of the Toll-like receptor family of innate immunity pattern-recognition receptors are abundant in the male rat reproductive tract. *Biol Reprod* 76: 958 – 964

Park B, Brinkmann MM, Spooner E, Lee CC, Kim YM, Ploegh HL (2008) Proteolytic cleavage in an endolysosomal compartment is required for activation of Toll-like receptor 9. *Nat Immunol* 9: 1407 – 1414

Pasparakis M (2009) Regulation of tissue homeostasis by NF-kappaB signalling: implications for inflammatory diseases. *Nat Rev Immunol* 9: 778 – 788

Peter ME, Kubarenko AV, Weber AN, Dalpke AH (2009) Identification of an N-terminal recognition site in TLR9 that contributes to CpG-DNA-mediated receptor activation. *J Immunol* 182: 7690 – 7697

Peterson MD, Mooseker MS (1992) Characterization of the enterocyte-like brush border cytoskeleton of the C2BBe clones of the human intestinal cell line, Caco-2. *J Cell Sci* 102(Pt 3): 581 – 600

Rhee SH, Im E, Riegler M, Kokkotou E, O'Brien M, Pothoulakis C (2005) Pathophysiological role of Toll-like receptor 5 engagement by bacterial flagellin in colonic inflammation. *Proc Natl Acad Sci USA* 102: 13610 – 13615

Sakamori R, Das S, Yu S, Feng S, Stypulkowski E, Guan Y, Douard V, Tang W, Ferraris RP, Harada A, Brakebusch C, Guo W, Gao N (2012) Cdc42 and Rab8a are critical for intestinal stem cell division, survival, and differentiation in mice. *J Clin Invest* 122: 1052 – 1065

Sato T, Mushiake S, Kato Y, Sato K, Sato M, Takeda N, Ozono K, Miki K, Kubo Y, Tsuji A, Harada R, Harada A (2007) The Rab8 GTPase regulates apical protein localization in intestinal cells. *Nature* 448: 366 – 369

Sato T, Vries RG, Snippert HJ, van de Wetering M, Barker N, Stange DE, van Es JH, Abo A, Kujala P, Peters PJ, Clevers H (2009) Single Lgr5 stem cells build crypt-villus structures *in vitro* without a mesenchymal niche. *Nature* 459: 262 – 265

Su L, Shen L, Clayburgh DR, Nalle SC, Sullivan EA, Meddings JB, Abraham C, Turner JR (2009) Targeted epithelial tight junction dysfunction causes immune activation and contributes to development of experimental colitis. *Gastroenterology* 136: 551 – 563

Tabeta K, Hoebe K, Janssen EM, Du X, Georgel P, Crozat K, Mudd S, Mann N, Sovath S, Goode J, Shamel L, Herskovits AA, Portnoy DA, Cooke M, Tarantino LM, Wiltshire T, Steinberg BE, Grinstein S, Beutler B (2006) The Unc93b1 mutation 3d disrupts exogenous antigen presentation and signaling via Toll-like receptors 3, 7 and 9. *Nat Immunol* 7: 156 – 164

Vereecke L, Sze M, McGuire C, Rogiers B, Chu Y, Schmidt-Supprian M, Pasparakis M, Beyaert R, van Loo G (2010) Enterocyte-specific A20 deficiency sensitizes to tumor necrosis factor-induced toxicity and experimental colitis. *J Exp Med* 207: 1513 – 1523

Vinderola G, Matar C, Perdigon G (2005) Role of intestinal epithelial cells in immune effects mediated by gram-positive probiotic bacteria: involvement of Toll-like receptors. *Clin Diagn Lab Immunol* 12: 1075 – 1084

Vlantis K, Wullaert A, Sasaki Y, Schmidt-Supprian M, Rajewsky K, Roskams T, Pasparakis M (2011) Constitutive IKK2 activation in intestinal epithelial cells induces intestinal tumors in mice. *J Clin Invest* 121: 2781 – 2793

Wang X, Kumar R, Navarre J, Casanova JE, Goldenring JR (2000) Regulation of vesicle trafficking in madin-darby canine kidney cells by Rab11a and Rab25. *J Biol Chem* 275: 29138 – 29146

Wells JM, Rossi O, Meijerink M, van Baarlen P (2011) Epithelial crosstalk at the microbiota-mucosal interface. *Proc Natl Acad Sci USA* 108(Suppl. 1): 4607 – 4614

Yao Y, Hong S, Zhou H, Yuan T, Zeng R, Liao K (2009) The differential protein and lipid compositions of noncaveolar lipid microdomains and caveolae. *Cell Res* 19: 497 – 506

Zeng X, Chauhan C, Hou SX (2010) Characterization of midgut stem cell- and enteroblast-specific Gal4 lines in drosophila. *Genesis* 48: 607 – 611

Zhang J, Stirling B, Temmerman ST, Ma CA, Fuss IJ, Derry JM, Jain A (2006) Impaired regulation of NF-kappaB and increased susceptibility to colitis-associated tumorigenesis in CYLD-deficient mice. *J Clin Invest* 116: 3042 – 3049

Zhou F, Rasmussen A, Lee S, Agaisse H (2013) The UPD3 cytokine couples environmental challenge and intestinal stem cell division through modulation of JAK/STAT signaling in the stem cell microenvironment. *Dev Biol* 373: 383 – 393